Geometric Magnetic Frustration in Crystal Lattices: Synthesis and Magnetic Characterization of Breathing Pyrochlore Candidates $CuAlCr_4S_8$ and $CuAlCr_4Se_8$

By

Matthew Pocrnic

A Thesis

Submitted to the School of Interdisciplinary Science

In Partial Fulfillment of the Requirements

For the Degree

Bachelor of Science

McMaster University

Bachelor of Science (2021) McMaster University

School of Interdisciplinary Science Hamilton, Ontario

TITLE: Geometric Magnetic Frustration in Crystal Lattices: Synthesis and Magnetic Characterization of Breathing Pyrochlore Candidates $CuAlCr_4S_8$ and $CuAlCr_4Se_8$

AUTHOR: Matthew Pocrnic

SUPERVISOR: Professor Graeme Luke

NUMBER OF PAGES: 49

Abstract

The breathing pyrochlore lattice is a relatively recently discovered variant of the extensively studied pyrochlore. Materials exhibiting this structure possess the chemical formula $AA'B_4X_8$ and form a lattice of interpenetrating corner-sharing tetrahedra of alternating sizes due to the differences in atomic radii of the A and A' atoms that occupy the neighbouring sites. The difference in tetrahedra size can be quantified by the breathing factor $B_f \equiv \frac{d'}{d}$. This lattice exhibits magnetic frustration as a result of its geometry, as the tetrahedral structure prevents all nearest neighbour interactions from being satisfied, and the introduction of the breathing factor breaks the symmetry of the nearest neighbour Hamiltonian, providing an arena for studying interesting magnetic interactions. Here, I present an experimental study of the breathing pyrochlore candidates $CuAlCr_4S_8$ and $CuAlCr_4Se_8$. I provide the procedure for synthesis using solid state techniques, as well as a structural analysis using X-ray diffraction and Rietveld refinement. I also perform a magnetic characterization of the samples using SQUID magnetometry, where M(H) and M(T) measurements are conducted. Through analysis of these measurements, I conclude $CuAlCr_4S_8$ forms a nearly pure breathing pyrochlore with no magnetic impurities and $B_f = 1.087$. This is the first reporting of this material. The sample undergoes a significant transition at $T_c \approx 26K$ which appears to be first order in nature and possibly antiferromagnetic. This material has a Curie-Weiss temperature $\theta_{CW} = -61.93K$. Analysis of $CuAlCr_4Se_8$ shows it forms a mixed site pyrochlore structure, with a small paramagnetic impurity $Cr_{0.68}Se \approx 2.5\%$. This material exhibits multiple characteristic temperatures and spin glass-like behaviour with $\theta_{CW} = 17.14K$.

Acknowledgements

I would like to thank Dr. Graeme Luke of the McMaster Physics Department for providing support and guidance over the duration of this project, and for making this thesis possible. Completing an experimental thesis during a pandemic was a challenge, yet I am extremely grateful to be amongst the few who were afforded the opportunity to conduct laboratory research despite the circumstances, and I am thankful for the experience and knowledge I have gained along the way. In addition, I would like to thank Ph.D. student Sudarshan Sharma for leading the investigation in the lab, as well as teaching me all of the methods and answering my many questions. Sudarshan made key experimental decisions over the course of this project which ultimately allowed for the discovery of a new material. I am very grateful for having had the opportunity to work with him.

Table of Contents

List of Figures

1 Introduction

The focus of this thesis is a phenomenon known as geometric magnetic frustration. This project resides in the field of experimental condensed matter physics, in which geometric magnetic frustration is a topic of much interest. Magnetism is a fascinating phenomenon in that it can be understood and appreciated by all at some level, yet its emergence and behaviour in materials is complex, and requires a quantum mechanical description. A quantum understanding of magnetic materials is important. Magnetism plays a large role in modern electronics, and exotic magnetic states may provide critical future applications, especially in the emerging field of quantum computation. As the field of quantum technology continues to advance, and the demand for quantum devices grows, a deep understanding of the quantum mechanical behaviour of solids will be of great importance. With this in mind, this project is an experimental search for interesting physics within a class of materials known as the breathing pyrochlores. This document will provide the background for this investigation, as well as introduce the system of study, and motivate the project. I then discuss the methods used for material synthesis, structural analysis, and magnetic characterization. I will then proceed to present the outcomes of each of these stages of the project. Finally, I conclude the document with a discussion about the implications of the gathered results, and mention avenues for future work and experiments on the subject.

2 Background and Theory

Magnetism is undoubtedly a very extensive and complex topic, especially when considering materials in condensed matter physics. With this in mind, the following sections serve not as a deep theoretical background, but as an interesting theoretical discussion to highlight various concepts that are discussed and investigated throughout this thesis. Along the way, I will motivate and quote notable results that will show their relevance in the experimental investigations that follow.

2.1 Origins of Magnetism in Materials and Magnetic Interactions

Magnetism is a strange phenomenon in that it is simple enough to be appreciated by a child placing magnets on a refrigerator, yet its complete description remained elusive until the 20th century. Classically, magnetism is described by the Maxwell equations. When these equations are uncoupled, second order differential equations are obtained, which famously take the form of wave equations [1]. When solved in the vacuum, one can immediately notice the wave speed is equal to the speed of light, and conclude that light is an electromagnetic wave. This beautiful emergence of c led to Einstein postulating that the speed of light is a universal constant and led to the advent of special relativity, ushering in modern physics. Magnetism seems to arise in nature in unintuitive ways: through changing electric fields and currents, and is often described with the mathematics of the curl. This may lead one to ask why magnetism exists in the first place? Interestingly, with only the theory of electrostatics, one can show that special relativity directly implies the existence

of magnetism (see Griffiths page 550 [1]). However, although intriguing, this story still does not tell us physically where magnetism originates. Magnetism cannot be a pure artefact of relativity due to the fact that our introductory example of the refrigerator magnet would be left unaccounted for. Magnetism originates quantum mechanically in materials due atomic spins (their constituent particle spins) and their interactions, as well as the motion of electrons forming microscopic currents (the latter of which we might have come to expect) [2]. A feature of critical importance to magnetism is the exchange interaction, which is a pseudo-force that arises purely as a result of how nature counts its particles [3]. The exchange interaction is a purely quantum phenomenon, with no classical analog. It arises as a result of the way nature presents itself in multiparticle quantum mechanics. Wavefunctions that have been found to describe symmetrical systems come as either fully symmetric or completely antisymmetric. If we are to consider a 2-particle wave function in position space, this means that there are only two ways to write it down:

$$|\Psi\rangle_{\pm} = \frac{1}{\sqrt{2}}\left(|\psi_a(r_1)\psi_b(r_2)\rangle \pm |\psi_a(r_2)\psi_b(r_1)\rangle\right) \qquad (1)$$

It is written as a superposition as the particles are identical, with the symmetric case representing bosons (particles with integer spin) and the antisymmetric case for fermions (particles with half integer spin) [3]. The reason they are indistinguishable is that in quantum mechanics it is meaningless to say “this” or “that” electron, in the language of quantum field theory, all of these particles are the excitations of their respective field. Of course, if we have the case where the two particles are different and truly distinguishable (such as a proton and electron) then the wave function is simply $|\Psi\rangle = |\psi_a(r_1)\psi_b(r_2)\rangle$. The

exchange interaction becomes apparent when we calculate the expectation value of the square of the separation between the particles described by equation (1), we obtain:

$$\langle (r_2 - r_1)^2 \rangle_{\pm} = \langle r^2 \rangle_a + \langle r^2 \rangle_b - 2\langle r \rangle_a \langle r \rangle_b \mp 2|\langle r \rangle_{ab}|^2$$

where $\langle r \rangle_{ab} = \int r\, \psi_a^*(r)\psi_b(r)dr$. The significance of this calculation comes in the $2|\langle r \rangle_{ab}|^2$ term, which is not present if the same calculation is carried out for a wavefunction describing distinguishable particles [3]. This means that identical fermions "live" further from each other than identical bosons, as dictated by the final term in the expression. It is almost as if a mysterious force repels fermions from each other and attracts bosons, yet there is no force in play here. The implications of this effect on magnetism in materials is immense. Solids, of specifically crystalline order, are comprised of identical bases of atoms that occupying lattice sites, and the fundamental unit of a crystal is the unit cell, which can be used to construct the entire solid by repeating in space [4]. Considering electrostatic interactions, particles of like charge minimize energy when they are far apart, and cost energy when they are close together [2]. Considering these particles are atoms that can be either bosons or fermions, depending on the sums of the spins of their constituent particles, through influencing the distances between atoms, the exchange interaction influences the structure of the solid. Furthermore, the exchange interaction plays a greater role in the magnetic behaviour when spin is added to the story. If the spinors $\chi_{\pm}$ are introduced to the symmetric and antisymmetric wavefunctions written in equation (1); $|\Psi\rangle_{\pm} = \frac{1}{\sqrt{2}}(|\psi_a(r_1)\psi_b(r_2)\rangle \pm |\psi_a(r_2)\psi_b(r_1)\rangle)\chi_{\pm}$ we notice that these wavefunctions represent the

singlet and triplet states respectively. Following Blundell [2], we write the effective Hamiltonian as:

$$\mathcal{H} = \frac{1}{4}(E_+ + 3E_-) - (E_+ - E_-)\boldsymbol{S_1} \cdot \boldsymbol{S_2}$$

where E and $\boldsymbol{S}$ represent the energy of the state and spin operator respectively. This Hamiltonian comes from the fact that $\boldsymbol{S_1} \cdot \boldsymbol{S_2} = -\frac{3}{4}$ for a singlet state where the total spin is S = 0 (spins are anti-aligned), and $\boldsymbol{S_1} \cdot \boldsymbol{S_2} = \frac{1}{4}$ for the triplet state where total spin S=1 (spins are aligned). The exchange integral J is defined half the energy difference between the two states:

$$J = \frac{1}{2}(E_+ - E_-) = \int \psi_a^*(r_1)\psi_b^*(r_2)\mathcal{H}\psi_a(r_2)\psi_b(r_1)dr_1dr_2$$

Given J and the Hamiltonian, notice that the spin dependent part of the Hamiltonian can be written $\mathcal{H} = -2J\boldsymbol{S_1} \cdot \boldsymbol{S_2}$. Now it is time to make the connection to magnetism. If the $J > 0$ then $E_+ > E_-$ which means that the state with the aligned spins, the triplet state in the case of spin half, is energetically favourable, and will present itself to minimize the Hamiltonian as all physical systems tend to minimize energy. In a crystal, this relates to the case of ferromagnetism, since by minimizing energy, spins align giving a net magnetic moment and magnetization. When the converse is true, and $J < 0$, we get the case of anti-aligned spins, hence, antiferromagnetism, with zero net magnetization of the crystal. This served to motivate the Hamiltonian that will be used to discuss magnetic interactions for the rest of the thesis. This was an example of the interaction between two indistinguishable quantum particles, but for a solid, we need to sum over all particles. For simplicity,

considering only nearest neighbours the Heisenberg model Hamiltonian can be obtained: $\mathcal{H} = -\sum_{ij} J_{ij} \boldsymbol{S}_i \cdot \boldsymbol{S}_j$, where Heisenberg spins are not confined to specific axes [2].

2.2 Phase Transitions

A critical feature of Heisenberg model Hamiltonians of the aforementioned form are phase transitions. While crucial to our understanding of solids, they are not at all obvious at first sight of the model, and can be difficult to show mathematically. An important and interesting scenario is a simplification of the more generic Heisenberg model called the Ising model. With this model, spins are confined along a locally defined axis and interactions are only between nearest neighbours. If we expand the inner product in the Heisenberg Hamiltonian we obtain: $\boldsymbol{S} \cdot \boldsymbol{S} = S_{ix}S_{jx} + S_{iy}S_{jy} + S_{ix}S_{jy}$. If the last term dominates, the spins are called Ising like. With this model, we are free to employ certain geometries and see how it behaves. With only spin up and spin down to consider this model seems rather simple, however, solving this system in even 2-dimensions is extremely difficult as was shown by Onsager's exact solution in 1944 [5]. Interestingly, even in this system that may seem contrived at first glance, Onsager showed through his exact solution that this model undergoes a phase transition at some critical temperature T_c. This means that at a given low temperature, a system of interacting spins will establish some form of long-range spin ordering. In addition, spins can physically be Ising like, Heisenberg like (about equal contributions of terms in $\boldsymbol{S} \cdot \boldsymbol{S}$), or XY like (in which they are confined to a plane where $S_{ix}S_{jx}, S_{iy}S_{jy}$ terms dominate) depending on the crystal field of the magnetic

atoms in the lattice [2]. This is important because as we will see, physical systems also exhibit phase transitions and spin ordering at specific temperatures. In light of the mathematical complexity of the problem, computer simulations such as the Monte Carlo are often employed for more realistic systems, such as the Heisenberg model, and can even be employed to include next nearest neighbours in the interactions, to further improve the accuracy of the solutions [6]. Approximate analytical methods such as mean field theory have also been developed to investigate the simpler cases of interacting systems. A notable mean field theory framework in spin systems is the Landau theory, in which the free energy of the system can be Taylor expanded in terms of an order parameter ϕ [7]:

$$f = a_0 + a_1\phi + a_2\phi^2 + \cdots$$

The concept of an order parameter is important, and differs across many physical systems. Following the name, it is a parameter that characterizes order in the system. In magnetic systems, a typical choice of this parameter is the average magnetic moment. For example, if we are investigating a ferromagnetic transition in the Ising model, the disordered state would be represented by $\phi = 0$ [7]. Further approximations, can be made and symmetries exploited in order to solve the system in this manner. For example, one can notice that in the Ising model, flipping all of the spins $\phi \to -\phi$ does not change the free energy of the system, allowing the odd terms to be dropped [7]. Since physical systems tend to minimize the free energy, when minimized, the remaining equation $f = a_2\phi^2 + a_4\phi^4$ (neglecting the influence of higher ordered terms) will have solutions for ϕ that are zero and non-zero, corresponding to ordered and disordered phases.

2.3 Geometric Magnetic Frustration and the Breathing Pyrochlore Lattice

This section is at the heart of this thesis, but it is not meant to serve as a literature review. Here, I will try to be brief and summarize the most important ideas for the investigation. Consider again the Ising model in two dimensions with antiferromagnetic nearest neighbour interactions. However, suppose we change the geometry of the system such that the lattice is composed of equilateral triangles rather than a square grid (see Figure (1)).

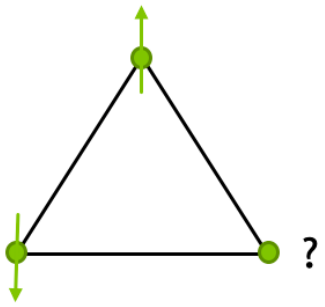

Figure 1: Ising spin antiferromagnet on a triangular lattice creates a simple frustrated system. The geometry prevents the nearest neighbour interactions from being simultaneously satisfied.

In this case, the positions and geometry do not alone give the full story. If the system spins interacted ferromagnetically, there would be no frustration present, but a net magnetic moment instead [8]. Frustration is also often defined as the inability for a system to find a unique ground state. In this simple example, there exists a threefold degeneracy of the ground state. Extensive ground state degeneracy leads to large zero temperature entropy and is characteristic of highly frustrated systems [9].

Examples of frustrated systems become more interesting in 3-dimensions, as given the increased richness of $\mathbb{R}^3$ compared to $\mathbb{R}^2$, there are many more potential lattices to realize, and more interesting physics to investigate. An interesting and extensively studied

3D lattice is that of the pyrochlore lattice, which is a lattice of interpenetrating corner-sharing tetrahedra that exhibits geometric magnetic frustration [9]. These are materials that follow the formula $A_2B_2O_7$, and the interpenetrating A and B sites can be seen in Figure 2.

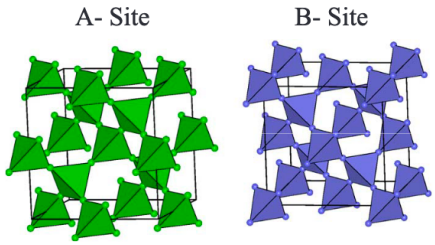

Figure 2 A schematic of the A and B site lattices of the pyrochlore oxide [9].

The corner sharing nature of the lattice gives it lower connectivity, resulting in higher degeneracy, which makes this lattice a highly suitable system for the study of frustrated states. This lattice has provided an arena for the study of interesting magnetic states including spin glass, spin liquid, and spin ice, depending on the magnetic ion. In the lattice, the A site, B site, or both sites can be occupied by magnetic ions. As well, this lattice has provided candidate materials for the observation of the experimentally elusive quantum spin liquid which has never been decisively observed [9]. Within these exotic states of magnetism, interesting phenomena arise. The spin ice state theoretically allows for magnetic monopole separation, providing a regime for the violation of the Maxwell equation $\nabla \cdot B = 0$ when the spin problem is mapped onto the lattice [10]. However, as these are not true monopoles, Maxwell's equations still hold in actuality. Next, the spin glass state represents an example of quenched random frustration, where the name spin glass comes from the analogous nature of structural disorder in chemical glass. In spin glasses, there is randomness in either the spin or position degrees of freedom, in that the

spatial ordering or the strength of the neighbouring interactions can be random [11]. At sufficiently low temperatures, these materials will exhibit spin-freezing, in which the spins "freeze" in a metastable disordered state that is not a ground state [11]. Onwards, the quantum spin liquid state theoretically arises when quantum fluctuations become large with respect to thermal fluctuations in a frustrated lattice, and strong enough to prevent ordering of spins. As a result, a state consisting of superpositions of spins simultaneously pointing in different directions emerges. A product of this state is mass many body entanglement, with coexistence of large spatial separation and large spin correlations [10]. It is important to investigate these materials, as these properties may have future applications, possibly towards the rapidly growing field of quantum information technology.

The breathing pyrochlore lattice is a variant of the pyrochlore lattice that possesses the chemical formula $AA'B_4X_8$. This is a modified version of the chemical formula AB_2X_4, which is that of the spinel, a material comprised of two A and B sublattices. The B sublattice takes the form of the pyrochlore lattice with interpenetrating corner-sharing tetrahedra, thus we require the atom at the B-site to be magnetic (have non-zero spin). Introducing A' into the chemical formula results in A-site sharing in the A sublattice, which takes the form of a diamond lattice. The breathing pyrochlore lattice is effectively obtained when site-ordering occurs at the A-site. If there is lack of ordering or mixing of the A-site, where the positions of A and A' are random, the material would be classified as a mixed site pyrochlore. In the breathing pyrochlore lattice, the interpenetrating tetrahedra in the B sublattice alternate in size due to the difference in atomic radii between the A and A' atoms, which orderly occupy neighbouring lattice sites. This leads to the contraction and expansion

of alternating tetrahedra that connect the magnetic ions at the B-site, known as a breathing modulation [12]. This allows one to define the breathing factor, which is the ratio between the tetrahedral edges of differing size: $B_f \equiv \frac{d'}{d}$. In comparison, the standard pyrochlore lattice would have a breathing factor of 1. The breathing modulation has significant implications on the magnetic behaviour of the solid. If the breathing factor is very close to 1, we may come to expect behaviour that is similar to that of a pyrochlore lattice, and if the breathing factor is too large the lattice will have large tetrahedral separation and will likely exhibit 4-spin physics, or local interactions at each small tetrahedron. The interesting domain is the midfield, in which breathing factor is just large enough for competing interactions to be significant. The pyrochlore oxide is described by the Heisenberg nearest neighbour Hamiltonian introduced earlier, however, the breathing modulation breaks the symmetry of this Hamiltonian, requiring an extra term as there are now two nearest neighbour exchange interactions:

$$\mathcal{H} = \sum_{i,j} J_{i,j}\, S_i \cdot S_j + \sum_{i,j} J'_{i,j}\, S_i \cdot S_j$$

This model can even be expanded (for more accuracy) to include second and third nearest neighbours. The third nearest neighbours provide another asymmetry, since J_{3a} is bisected by an B site while J_{3b} is not (see Figure 3) [13].

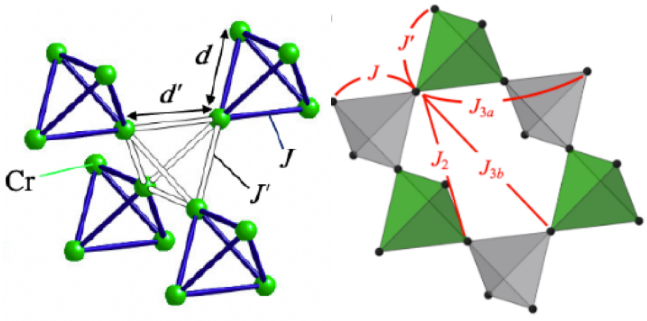

Figure 3 A) (left) a diagram of the breathing modulation with chromium at the B site [12] and B) (right) a diagram of the second and third nearest neighbour interactions that can be included in a more complicated minimal model Hamiltonian [13]

To the best of my knowledge, these materials have only been synthesized with Cr at the B site which has S=3/2. This lattice may allow for the study of interesting physics, such as competing short and long range magnetic interactions in ways that are not yet well understood.

2.4 Curie-Weiss Law

An important feature of magnets, especially those that are geometrically frustrated, is the temperature dependence of the magnetic susceptibility. The magnetic susceptibility is defined as $\chi = \frac{M}{H}$ where M is the magnetization or magnetic moment per unit volume, and H is the auxiliary magnetic field, or the magnetic field that is typically controlled when applied in experiments. The typical B field in magnetism is defined here as the resultant field due to the combined effects of the magnetization auxiliary field, related by the equation $H = \frac{1}{\mu_0}B - M$ [1]. The magnetization can also be defined as magnetic moment per gram or per mole of a sample, but more will be said about this later. The Curie-Weiss

law for the susceptibility of a solid in a small external field is the following (for derivation, see section 5.2 in [2]):

$$\chi^{-1} \propto T - \theta_{CW}$$

This law typically applies to ferromagnetic, antiferromagnetic, and paramagnetic systems in the region where $T > T_C, T_N$, where T_N is the Néel temperature which serves essentially the same purpose as the critical temperature for a ferromagnet, in that it is the temperature below which antiferromagnetic order is achieved. This law, however, does not apply in systems dominated by diamagnetism, in which the susceptibility is often constant [2]. If experimental data is used to plot inverse susceptibility vs temperature, the region in which the plot is linear is called the Curie-Weiss region. In terms of temperature scales used in experiments, the linear region is often in the high temperature regime between 100-300K. Conceptually, as temperature decreases, the amount of thermal fluctuations in the lattice decreases, therefore, the lattice spins are more easily influenced by the small constant external field, and hence susceptibility and temperature are inversely related. θ_{CW} is the Curie-Weiss constant and characterizes the sign and strength of the interactions ($\theta_{CW} > 0$ for ferromagnetism, $\theta_{CW} < 0$ for antiferromagnetism, and $\theta_{CW} = 0$ for a paramagnet). When a material is frustrated the magnitude of θ_{CW} is large and the critical temperature in which spin freezing or ordering occurs is small. This makes it convenient to define a frustration parameter to characterize the degree of frustration in the system: $f \equiv \frac{|\theta_{CW}|}{T_C}$ [14].

It is also common to introduce a constant of proportionality and write the law in the following form: $\chi = \frac{C}{T-\theta_{CW}}$ where $C = \frac{N_A g^2 S(S+1)\mu_B^2}{3k_B}$ is the Curie constant. Here g is the

Landé g-factor, S is the spin, and μ_B is the Bohr magneton. The constant also includes Avogadro's number and the Boltzmann constant. It is also common to rewrite this in terms of an effective magnetic moment for the material $\mu_{eff}^2 = g^2 S(S+1)$. If a Curie-Weiss curve is constructed using experimental data, the Curie constant is characterized by the slope of the plot. Therefore, one can calculate the effective moment of a material in the following way: $\mu_{eff} = \sqrt{\frac{3k_B C}{N_A}}$ where the effective moment has units of the Bohr magneton. In the later sections, I will calculate both μ_{eff} and θ_{CW} for the materials studied in this thesis.

2.5 System of Interest

The breathing pyrochlore represents the system of interest in this thesis. Over the course of this project, the synthesis of many materials thought to exhibit the breathing pyrochlore structure were attempted. The list of materials includes $CuGaCr_4O_8$, $CuInCr_4O_8$, $LiGaMn_4O_8$, $LiGaSc_4O_8$, $CuAlV_4S_8$, $CuAlCr_4S_8$, and $CuAlCr_4Se_8$. The majority of these materials were synthesized during this project, while some were older samples synthesized by the group which were re-fired at higher temperatures. The breathing pyrochlore appears to be a structure that is experimentally difficult to realize, in that I saw little success with the majority of these materials, not including $CuAlCr_4S_8$, and $CuAlCr_4Se_8$. For the rest of the materials, no pure phase of either the breathing pyrochlore or mixed site pyrochlore was obtained. The results of our reactions were commonly mixed arrangements of compounds involving combinations of some, but not all of the atoms in the formula. Therefore, our

reactions were producing a mixture of materials that are not of interest. Without a pure phase of a material, meaningful magnetic analysis cannot be done. During the mid-point of the project, the focus was switched from oxides to sulfides and selenides, and thus the remainder of the thesis focuses explicitly on $CuAlCr_4S_8$, and $CuAlCr_4Se_8$. This choice was made due to some recent success in synthesizing these compounds [15,16], as well as theoretical interest in that replacing O with S or Se may suppress nearest neighbour interactions with respect to further neighbour interaction, leading to potential observation of interesting physics [13].

3 Experimental Methods

3.1 Solid State Synthesis

All of the materials synthesized over the course of this thesis, other than $CuAlV_4S_8$, were attempted to be synthesized using the solid-state method, sometimes called the ceramic method. This method is unique as it allows for the reaction of solids to form polycrystals without a change in state, using powders as the reactants [17]. High purity powders (~99.97%) were obtained from Alfa Aesar. Given the fact that all of these elements that comprise $CuAlCr_4S_8$ and $CuAlCr_4Se_8$ are stable in their pure form, the reactions to produce these materials were very straightforward. Often these powders did not tend to contain pure elements, as they are unstable or highly reactive (ex: Li), in which case they came in oxides. In these cases, sometimes the procedure first involved the synthesis of a precursor. Onwards, the powders were weighed in stoichiometric amounts on a scale with sensitivity

on the order of milligrams, then thoroughly mixed using a mortar and pestle. This mixing was usually done for a period of approximately 20 minutes. The total mass of each sample prepared was 2g. The resultant powder was then pressed into a pellet. This was done using a metal die and a hydrostatic press. The next step in the ceramic method is applying high temperature to the sample by placing it into a furnace. Since the reaction occurs entirely in the solid state, large amounts of energy are required to overcome the lattice energy, such that an atom can diffuse to a new lattice site [17]. This diffusion rate is what governs the rate of reaction. The rate is slow, which explains the need to press the material into the pellet; to increase connectivity in the material. Despite being very fine, each powder particle contains many atoms, therefore, the mixing increases the solid-solid interface between the different elements, and the packing decreases the distance between the atoms, thereby increasing the rate of diffusion in the lattice. In the solid state, reactions only occur on the interface between two powders, therefore, the surface layer first reacts and then more atoms diffuse from the bulk material through this interface, allowing the reaction to proceed [17]. These reactions occur on the order of days, and although applying high temperature increases the rate, due to the reaction occurring only at interfaces, the atoms typically do not diffuse into the desired structure after the first anneal. The pellet must be taken out, broken up, mixed (at which point we carry out XRD to analyze the purity), and placed back into the furnace. Each time this is done, the purity of the desired phase tends to increase. When it comes to $CuAlCr_4S_8$ and $CuAlCr_4Se_8$, the pellets must first be sealed in a quartz tube, which is first purged with Argon gas (inert) and then evacuated before being sealed through melting the open end with a torch. This is due to the fact that at high

temperature, Sulfur and Selenium become volatile and can be lost, which would alter the stoichiometry. Using a quartz tube limits the temperature of the furnace to 1100°C, since the tube melts at around 1150°C. This was not a limitation of our experiment. The limiting factor associated with this method is that only polycrystalline compounds can be synthesized. In order to form a single crystal, special furnaces such as the floating zone or Bridgman techniques must be used. Despite the fact that the Luke Group specializes in these techniques, the fact that S and Se are volatile prevents these methods from being utilized.

3.1.1 Experimental Procedure

In terms of specific cycles and temperatures, for the first anneal of $CuAlCr_4S_8$ was heated to 400°C at 75°C/hr, and ramped at 33.3°C/hr until reaching 1000°C which was held for 72hrs. The sample was then cooled at 100°C/hr until reaching 700°C when it was quenched at room temperature. After crushing and mixing with the mortar and pestle, the sample was packed again into a pellet and placed into the furnace already at 700°C. This was not particularly chosen, there were problems cooling the furnace at the time. The sample was heated to 1100°C for 72hrs and quenched again at 700°C with 100°C/hr ramping and cooling again. For $CuAlCr_4Se_8$, the sample was heated to 900°C for 48hrs at 100°C/hr ramping and cooling. This was done twice, with no quenching and the same intermediate mixing steps.

The other compounds which did not form a single-phase material followed a similar prescription. $LiGaSc_4O_8$ was a sample previously prepared by the group that was re-fired

at a higher temperature. The thought was that higher temperatures may be required to realize the breathing phase, but this was unsuccessful. $CuGaCr_4O_8$, $CuInCr_4O_8$, and $LiGaMn_4O_8$ were all attempted with the solid-state method with no success. The former two compounds were also arc melted in attempt to react all of the reactants and form a single-phase compound, however, this was also unsuccessful. Finally, $CuAlV_4S_8$ was attempted with solid metals/pieces instead of powders (based on lab supply). These pieces were cut and weighed, and then melting was attempted in the furnace, which was unsuccessful. The rest of the thesis will focus on $CuAlCr_4S_8$ and $CuAlCr_4Se_8$, as much success was found in these compounds.

Figure 4: Pressed pellets of $CuAlCr_4S_8$ (left) and $CuAlCr_4Se_8$ (right) before the first anneal.

3.2 Crystal X-Ray Diffraction and Rietveld Refinement

In order to analyze the structure of the prepared polycrystals, X-rays are used to probe the internal atomic plane structure of the material. This method works based on the Bragg law: $2d \sin\theta = n\lambda$ and the fact that the wavelength of X-rays are comparable to the interplanar spacing within crystal lattices [4]. The derivation of this law comes from geometrical

optics. When the X-rays are incident on parallel atomic planes, diffracted beams only emerge from the structure when the reflected beams incident on each plane interfere in a constructive manner. This occurs when the path length difference is equal to an integer multiple of the wavelength. In reality, Bragg conditions are satisfied only at certain angles of θ when many planes contribute to the reflected beam. This is because in reality each crystal plane tends to reflect ~10^{-3}-10^{-5} times the intensity of the incident beam, so the number of planes required to form a detectable beam is inverse of this order [4]. It is therefore clear that the usefulness of the Bragg equation relies on the fact that lattices exhibit periodicity by definition. For a geometric interpretation of the Bragg law, see Figure 5.

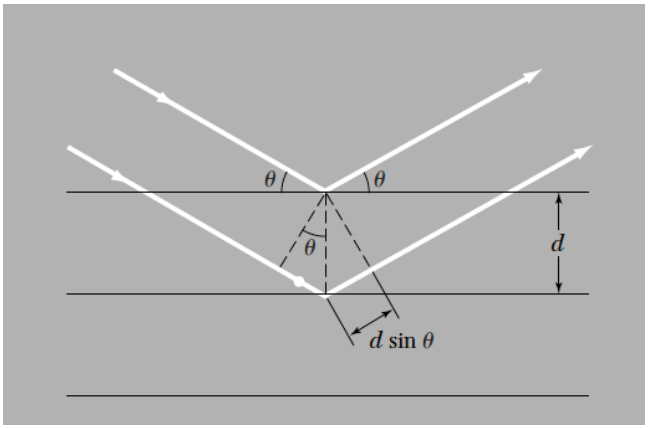

Figure 5: A geometric depiction of the Bragg condition with interplanar spacing d [4].

Whether or not the Bragg condition is satisfied depends on the orientation of the atomic planes in the crystal and thus the Miller indices (hkl) used to describe them. The mathematics of periodicity is Fourier analysis. Transforming to Fourier space allows one to refer to the reciprocal lattice, which yields another condition for X-ray diffraction:

$$\boldsymbol{k} \cdot \left(\frac{1}{2}\boldsymbol{G}\right) = \left(\frac{1}{2}G\right)^2$$

where $\boldsymbol{k}$ is the wavevector of the incident beam and $\boldsymbol{G}$ is a lattice vector in reciprocal space (see [4] for derivation). Constructing Wigner-Seitz cells in the reciprocal lattice creates what is known as a Brillouin zone, which geometrically gives the set of all wavevectors that will satisfy the Bragg condition.

In terms of employing this method in the lab, the PANalytical X'Pert Pro powder X-ray diffraction machine was utilized. This method involves obtaining powered samples, often from annealed pellets (broken up using the mortar and pestle) to determine the phase obtained through heating in the furnace. Small amounts of powder are placed on a single crystal silicon disk, that does not satisfy a Bragg condition over the range of rotation of the sample arm and therefore does not produce a background signal. This disk is coated in toluene so that the powder adheres to it for the duration of the measurement. It is important to use powders, that is polycrystalline samples. Due to the random orientations of the crystal planes in these samples, it is overwhelmingly probable that all possible Bragg conditions will be satisfied, while for a single crystal, only certain peaks will be pronounced. Once the sample disk is loaded into the machine, the sample tilts with respect to an incident X-ray beam, as well as it slowly rotates to obtain good averaging over the sample. To produce X-rays, the copper anode inside the machine is hit with electrons, which then ejects an electron out of the K-shell of the copper. A high energy electron then falls to the lower level to replace the K-shell electron, emitting an X-ray photon in the process [18]. This Cu Kα source is used to produce an incident of beam on the powder of

characteristic wavelength 1.5418×10^{-10}m. Rays diffracted by the powder that satisfy the Bragg condition then travel to the detector, where the machine registers a count. Over the course of the measurement, the powder X-ray diffraction machine produces a plot of intensity (counts) vs angle 2θ. The reason this method plots 2θ is because this is the angle between the incident beam and the detector. We do not plot θ since experimentally, this angle is unknown. This is due to the fact that we have a polycrystalline sample with atomic planes randomly oriented.

One this plot is obtained, I used HighScore Plus software to compare the diffraction to known profiles in the data base. This allowed for a quick understanding of the present phase of the sample, and the rapid identification of any impurities present. This step usually determined whether another anneal was required. After multiple anneals ion the furnace, and the sample appeared rather pure, the next step I carried out was a Rietveld refinement. This is a least-squares fit method that was done using Full Prof software. The method involves refining parameters such as lattice parameters, atomic and Wykoff positions, occupation number, background and scale of a known diffraction profile to fit the measurement collected. Once this process was complete, one of the outputs is a crystal information file that is refined the measured parameters of the powder. Using Vesta software, structural analysis visualization can be conducted. Through this method, unit cell volume, theoretical density, and breathing factor were calculated for some samples.

3.3 Magnetic Characterization with SQUID Magnetometry

Once samples had been synthesized, and the desirable phase purity was obtained, the next step in this investigation was understanding the magnetic behaviour of the materials. To do this, we utilized Quantum Design's Magnetic Property Measurement System (MPMS), which employs a Superconducting Quantum Interference Device (SQUID) to make extremely sensitive magnetic measurements. The MPMS can generate large magnetic fields (up to 7 Tesla), and measure changes in those fields (due to sample magnetization) up to 14 orders of magnitude smaller [19]. In this thesis, we use this device for two measurements: studying the magnetization as a function of applied magnetic field at a constant temperature which is often denoted M(H), and studying the magnetization as a function of temperature in a constant external field M(T). To do this, a very small amount of the sample (~mg) was placed in a capsule inside of the sample chamber tube and lowered into the chamber of the machine. The MPMS contains 4 superconducting detection coils that can be observed in Figure 6. These coils all form a closed loop, and the coils are arranged such that the net magnetic flux through the loop due to an externally applied magnetic field is 0. Therefore, the superconducting detection loops are only sensitive to the field produced through the magnetization of the sample [19].

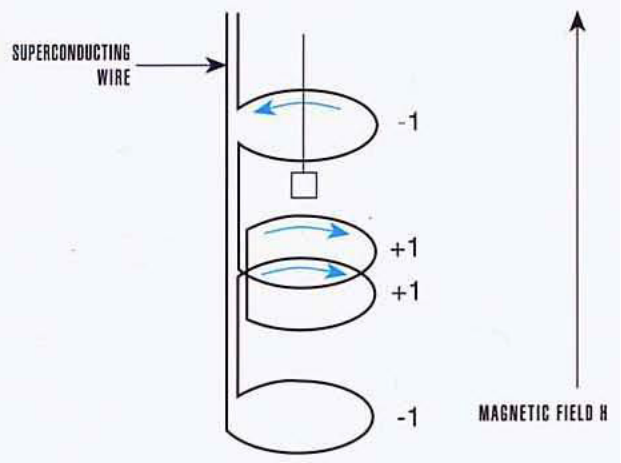

Figure 6: A diagram of the detection coils inside of the MPMS chamber, with the sample (square) being transported through the coils, and the direction of the current is shown in blue [19].

The SQUID is coupled to this loop and utilizes the Josephson effect (involving the quantum tunneling of paired electrons called Cooper pairs) to make extremely sensitive measurements of the magnetic flux [20]. After measuring the flux due to the sample at different positions, and averaging, the SQUID reports the magnetic moment of the sample in electromagnetic units (emu) [19].

Another important aspect of super conductance are the solenoidal coils (not to be confused with the detection coils) that are used to produce the field. In the case of an M(T) measurement, a constant current source does not need to be applied to produce the external field. The circuit is opened through heating of a small portion of the loop, which disrupts the superconducting phase. The current is then slowly adjusted with an external source to produce the desired field, at which point the heating is halted and the superconducting circuit closes [19]. In the absence of resistance, this magnetic field will persist at a constant

value for, in a theoretical sense, an infinite amount of time. Therefore, the fascinating nature of superconducting materials allows for extremely precise and constant fields to be applied, as well as for accurate measurements to be made.

The final important topic regarding the MPMS is temperature. This is important not only to maintain the superconducting phase of the detection and solenoid coils, but to observe phase transitions in the samples. In this project liquid He^4 was used to cool the sample down to ~2K, as well as it is used to cool the SQUID magnet. The MPMS also allows for the installation of an auxiliary He^3 cryostat which can be utilized to achieve even cooler temperatures, however, given that transitions were observed before this point, this was not performed.

4 Results and Discussion

4.1 Refinement and Structural Analysis

4.1.1 $CuAlCr_4Se_8$ Structural Analysis

With each attempt at synthesizing $CuAlCr_4Se_8$, the breathing phase could not seem to be realized. The material formed a mixed site pyrochlore in the space group $Fd\bar{3}m$, meaning the Cu and Al atoms that share the A site are not ordered in comparison to the breathing phase which has A site ordering. We also noticed that not all of the peaks could be explained simply by the known profile of $CuAlCr_4Se_8$, and that there was in fact an impurity $Cr_{0.68}Se$ $\approx 2.5\%$. In light of this, the stoichiometry was adjusted to include excess Al and Cu,

however, this did not seem to solve the problem within the timeline of the project. This is by no means an experimental failure, as this is simply the structure Nature chooses for this compound. Perhaps it will be possible to realize the breathing phase in this material in the future if different preparative methods are employed. Additionally, there were also complications with the Rietveld refinement when attempting to refine the data using the diffraction profile reported in [21] for unknown reasons. Instead, the structure was refined using a similar spinel $CuCr_2Se_4$. With this structure and the impurity, there was a good fit of the data (see Figure 7).

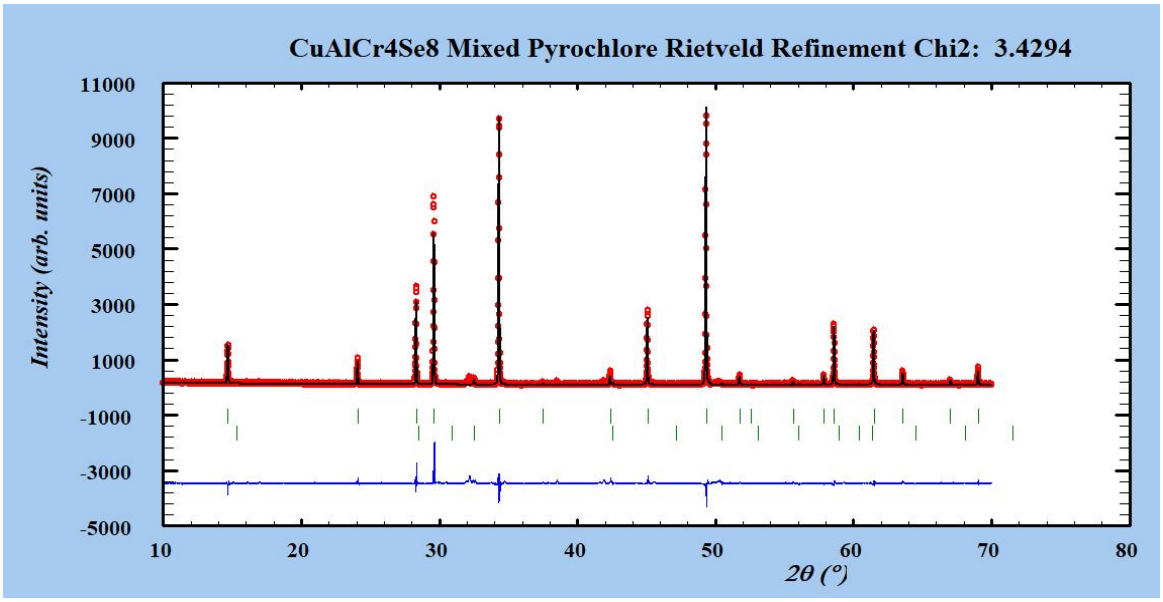

Figure 7: Rietveld refinement of the X-Ray diffraction profile of $CuAlCr_4Se_8$. The red points indicated the counts recorded by the PANalytical, with the black profile representing the refined fit. The blue set indicates the background, and the green lines indicate points at which a Bragg condition is satisfied. There are two series of green lines, the upper for $CuAlCr_4Se_8$ and the lower for the impurity Cr0.68Se. Good fit shown with chi squared = 3.4294.

The A site mixing made it difficult to realize the unit cell and conduct a structural analysis in using Vesta since the copper and aluminum atoms have essentially random positions. Here, no meaningful calculations could be completed since there is no breathing factor for this material.

4.1.2 $CuAlCr_4S_8$ Structural Analysis

The situation for $CuAlCr_4S_8$ is much more interesting compared to the selenide sample. When conducting the refinement of this sample, I experienced the same difficulty with the diffraction profile reported in [21], as was the case with the previous sample. However, we realized that this material forms the breathing phase or the structure described by space group $F\bar{4}3m$. This is indicated by the presence of extra peaks in the X-ray diffraction profile of $CuAlCr_4S_8$ which do not appear in that of the selenide material. These small peaks occur at $2\theta \approx 18,41$ and are visible in Figure 8 below. To the best of my knowledge, this is a novel breathing pyrochlore and the first reporting of this material. It is important to note, however, that this phase may have been obtained in [21], and technological limitations at the time prevented accurately determining the structure. Limitations could also explain the difficulties with refining these files. Since there is no existing diffraction profile for this breathing pyrochlore, given that it is novel, we used the diffraction profile data of another breathing pyrochlore $LiGaCr_rO_8$ reported in [12] to conduct the Rietveld refinement (see Figure 8).

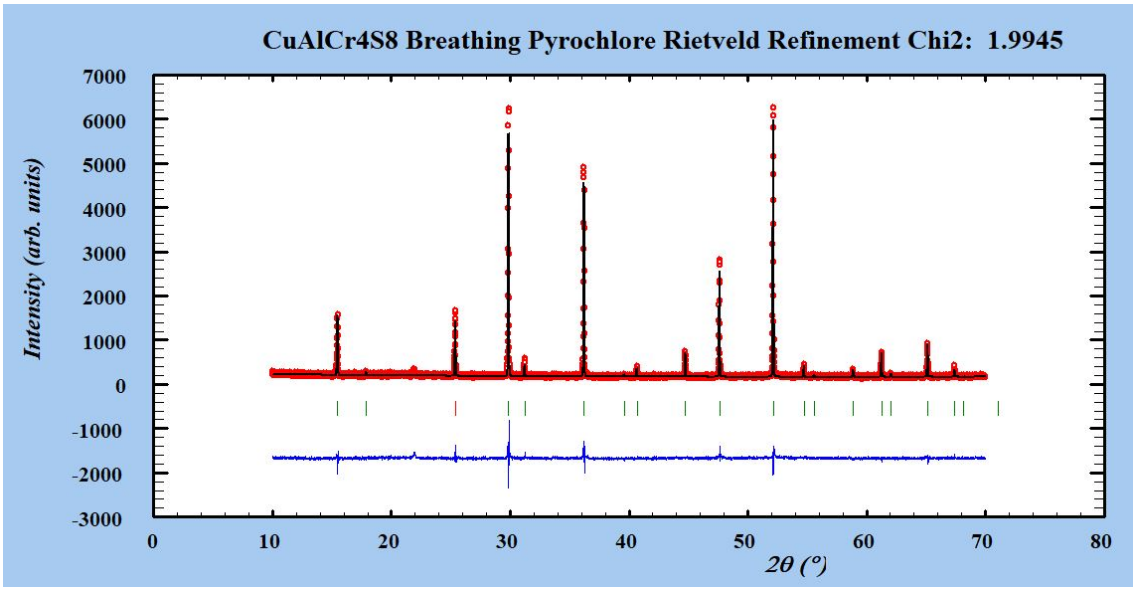

Figure 8: Rietveld refinement of the X-Ray diffraction profile of $CuAlCr_4S_8$. Very good fit shown with chi squared = 1.9945.

The fit obtained is nearly entirely perfect, with only a small impurity peak at $\theta \approx 22$, which corresponds to pure sulfur (determined through database peak matching using HighScore Plus). This is not a concern, as elemental sulfur is non-magnetic and thus will not interfere with the magnetic characterization of the sample.

Given that the material formed in the desired phase, I further investigated the structure using Vesta software. Vesta uses the new refined parameters within a crystal information file to generate the structure of the unit cell. The general structure calculated with Vesta can be seen in Figure 9A. However, this general structure showing the bonds does not illustrate the interactions of interest. I am interested in how the breathing phase affects the nearest neighbour S=3/2 chromium atoms which participate in the interaction Hamiltonian.

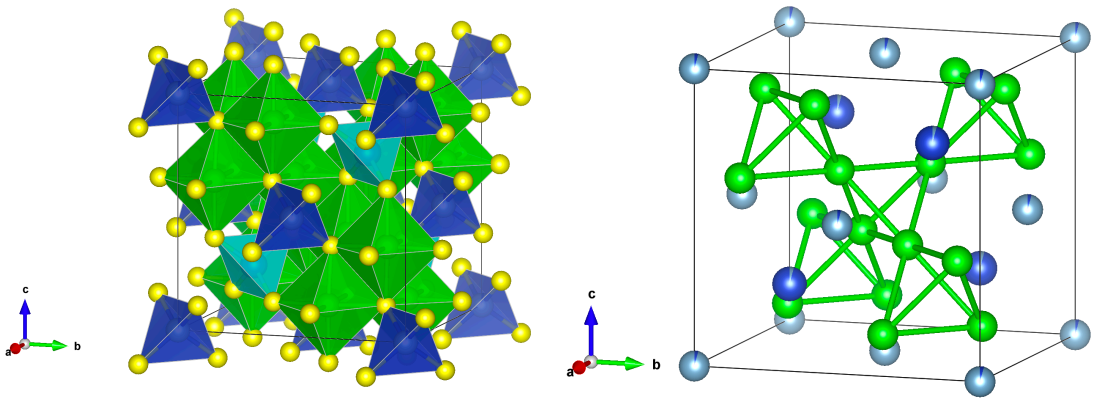

Figure 9 A) (left) The full crystal structure of $CuAlCr_4S_8$ with tetrahedra showing all nearest neighbour sulfide bonds. Sulfur in yellow, chromium in green, copper in dark blue and aluminum in light blue. B) (right) the same crystal structure with sulfur atoms supressed and tetrahedra connecting nearest neighbour chromium atoms. Due to the ordered A site sharing, the central tetrahedra is smaller than the other 4 in this unit cell.

Therefore, I created a new figure by suppressing the S atoms and all bonds in the lattice. I then programmed Vesta to bond all chromium atoms to all other chromium atoms within a 3-3.7 Angstrom distance. This range was determined essentially through predictions based on bond distances I measured in the lattice. The new structure can be seen in figure 9B. Using this structure, I was able to calculate the breathing factor $B_f = 1.087$, as well as the unit cell volume $V = 973.7$ Å^3, and the theoretical density $d = 3.786 g/cm^3$. The latter of which was done by counting the atoms and multiplying by atomic masses, where counting was done such that number of atoms that share faces and corners were divided by 2 and 8 respectively. This breathing factor is interesting as it appears to be one of the largest of what has been seen in breathing pyrochlore sulfides. However, it is still in that region that is not too much greater than 1. $LiGaCr_4S_8$, $CuInCr_4S_8$, and $LiInCr4S_8$, are the breathing phase sulfides that I am aware of, and they have breathing factors of approximately 1.07, 1.06, and 1.09 respectively [16]. These values are approximate due to the fact that in [16], values of d and d' are presented in a figure with numerical ranges, of which I interpreted.

In comparison, the breathing pyrochlore oxide $LiGaCr_4O_8$ (material data used to refine the sample) has $B_f \approx 1.036$ [12], which is significantly smaller than the sulfides. On the opposite end of the spectrum, $Ba_3Yb_2Zn_5O_{11}$ is an example of a material with a large breathing factor $B_f \approx 2$ [22]. Therefore, we might expect our material to behave similarly to $LiInCr_4S_8$, given that it shares a similar breathing factor and they have the same magnetic ion in chromium.

4.2 Magnetic Behaviour

4.2.1 $CuAlCr_4Se_8$ Magnetic Characterization

The magnetic study of this sample revealed some strange and unexpected behaviour. At the point time when sample was placed in the SQUID for measurement, the slight impurity present in the sample was not well understood in that we did not realize it was magnetic. When this sample was cooled in a constant external field, compared to cooling in zero external field, we saw drastically different behaviour (see Figures 10 and 11).

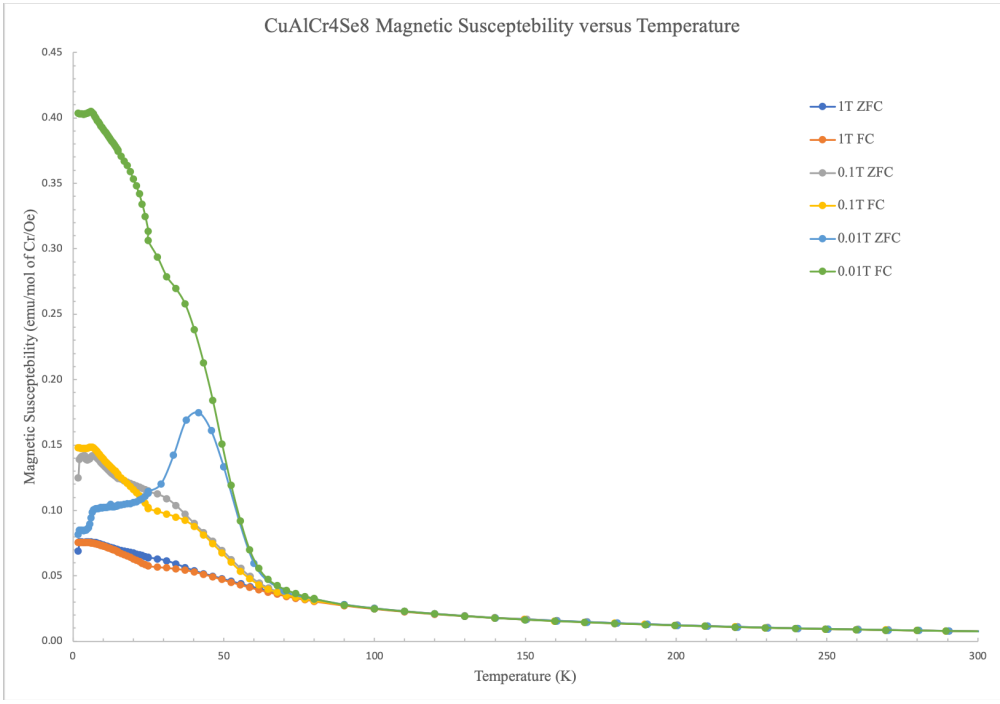

Figure 10: A plot of the magnetic moment as a function of temperature for CuAlCr4Se8 with both of the field cooled and zero field cooled series shown for multiple values of applied field.

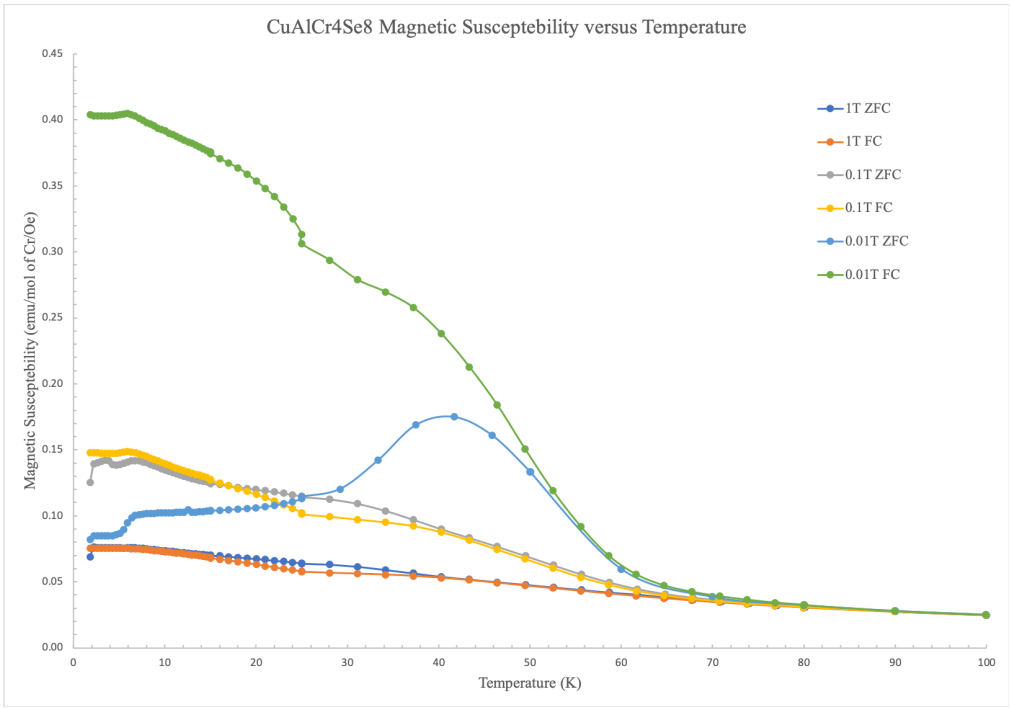

Figure 11: The same series shown as in the previous figure with the x-axis scale enlarged.

There is plenty going on with this sample, and it is difficult to make any significant conclusions from this data. The first thing to note is that it appears there are 2 or possibly 3 transition temperatures, and none of the transitions appear to be attributable to the impurity ($Cr_{0.68}Se \approx 2.5\%$). This material has an irreversibility temperature at $T_{irr} = 15K$ [23], and at this point we do not see a kink in the curve. In terms of the transition temperatures present, the first irreversibility temperature in our data occurs at $T_{irr} \approx 52K$. After this temperature, the field susceptibility is hysteretic in that the behaviour is different depending on if the material was field-cooled or zero-field-cooled. We also see potential spin freezing occurring here, indicating spin glass-like behaviour. The magnetic behaviour is extremely hysteretic in the lowest field which is interesting. Here, however, the impurity may have a contribution since the FC $Cr_{0.68}Se$ curve does behave paramagnetically at low temperatures [23]. There also seems to be some sort of transition occurring around $T_2 \approx 7K$, that is more pronounced in the smaller fields, and nearly invisible in the largest field. This could potentially be characteristic of a second order phase transition (given that it is smooth), which is possibly antiferromagnetic in nature. Around 25K, there may be another characteristic temperature, as is most evident in the 0.01T FC series. However, we must be cautious with this point since the measurement rate also changed in this neighbourhood. Therefore, the apparent kink may just be an artefact of the measurement. Small amounts of chromium sulfide impurity are also common in successful attempts to synthesize breathing pyrochlore sulfides [16], and this makes the study of our Sulfide compound even more interesting, given the absence of a magnetic impurity.

Further, I also plotted the inverse susceptibility of this curve and conducted a Curie-Weiss fit (see Figure 12).

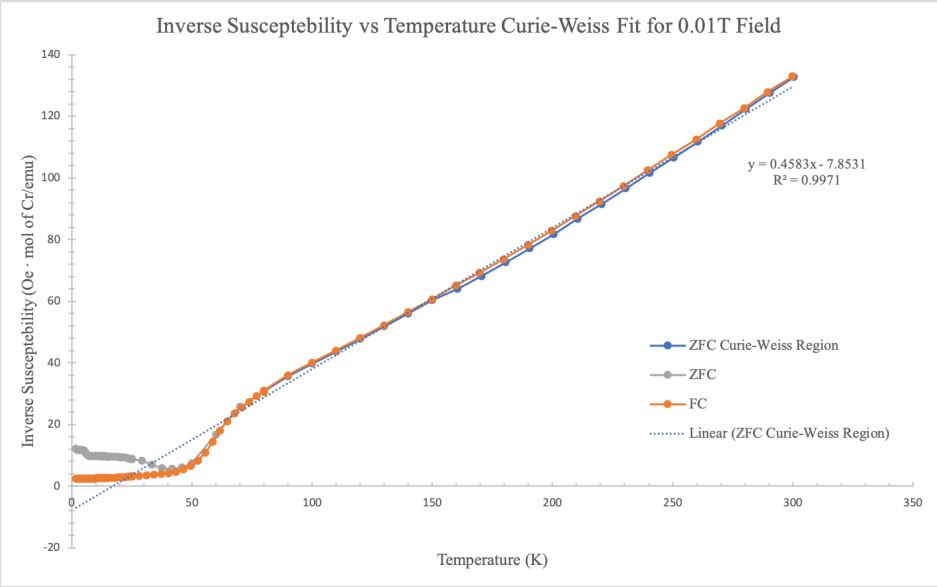

Figure 12: Plot of inverse susceptibility vs temperature in a 0.01T field with a Curie-Weiss fit of the linear region.

From this plot, I was able to calculate $\theta_{CW} = 17.14K$ and $\mu_{eff} = 0.605\mu_B$. Since this Curie-Weiss temperature is low and positive, I believe it may be indicative of competing antiferromagnetic and ferromagnetic or ferrimagnetic interactions, with one of the latter being more dominant. This, along with the spin glass behaviour is not too unexpected in our material given the fact that there is site mixing. This implies that the chromium interaction environment is somewhat random, and competing interactions and frustration are expected.

4.2.2 $CuAlCr_4S_8$ Magnetic Characterization

The magnetization data of $CuAlCr_4S_8$ is even more interesting, as it appears unhindered by magnetic impurities. There were existing concerns regarding the very small impurity peak at $\theta \approx 22$, but HighScore Plus software was used to confirm that this was purely sulfur, and would not interfere with measurement. Frist, let us consider a M(H) measurement of the sample (see Figures 13 and 14).

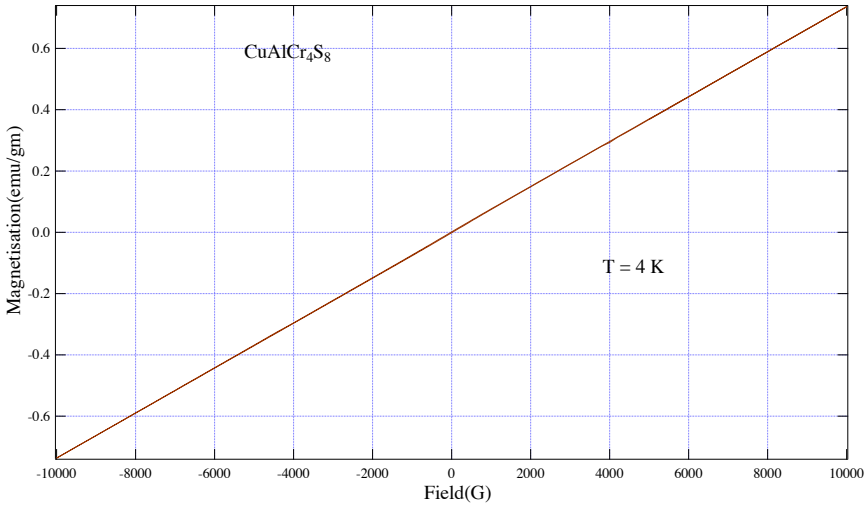

Figure 13: Magnetization of $CuAlCr_4S_8$ as a function of external field strength at constant temperature T=4K.

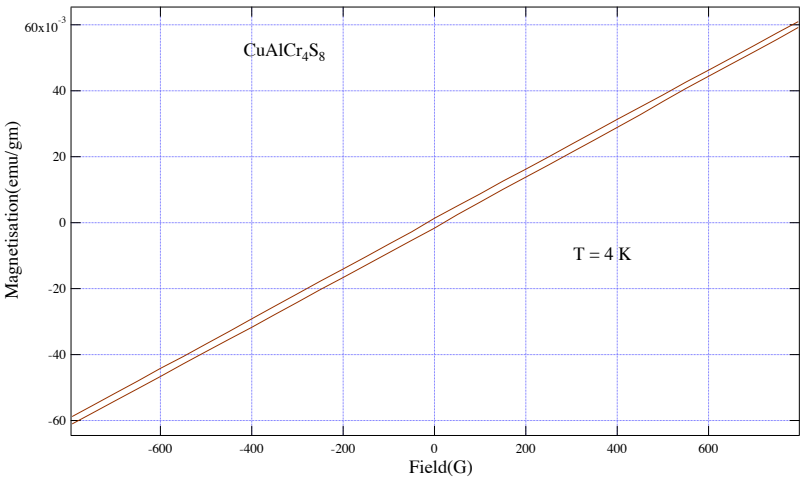

Figure 14: Magnetization of CuAlCr4S8 as a function of external field strength at constant temperature T=4K, with x-axis scale enlarged.

In these plots we see that there exists almost no irreversibility, with only a slight separation between the two linear sets that only becomes noticeable when the scale of the x-axis is magnified. Given that this minor separation is uniform, there is no presence of hysteresis that is concerning for temperature dependent susceptibility measurements. This is also likely attributable to the superconducting magnet in the SQUID itself. There is also no spin saturation that occurred over the course of the measurement. Going forward, it may be of interest to measure this sample in larger applied fields in order to see where this saturation occurs. This would be the point at which the sample is fully magnetized (serving as a maximum), and all the spins are contributing to the measured magnetization.

Next, we conducted an M(T) measurement. This was done for external fields of 0.01T, 0.1T, and 1T, each of which ZFC and FC data sets were collected. The SQUID gives values of the moment in emu, and following what appears standard in the literature, I calculate the magnetization in units of emu/mole of magnetic material. Then dividing by

the applied external field, I obtained plots of susceptibility with respect to temperature (see Figures 15 and 16).

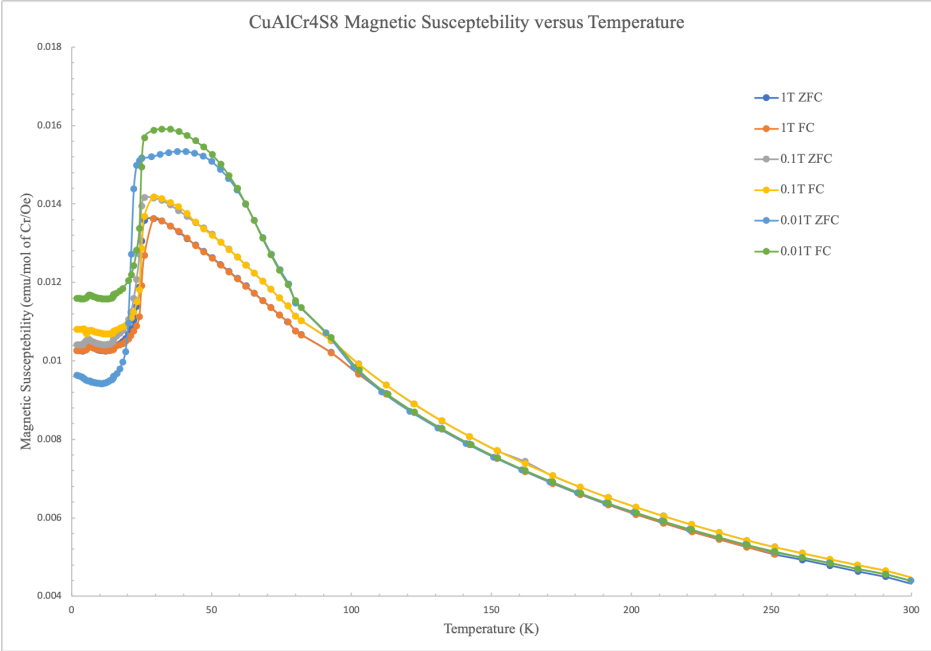

Figure 15: Plot of magnetic susceptibility of CuAlCr4S8 with respect to temperature, showing multiple series at different fields and cooling procedures.

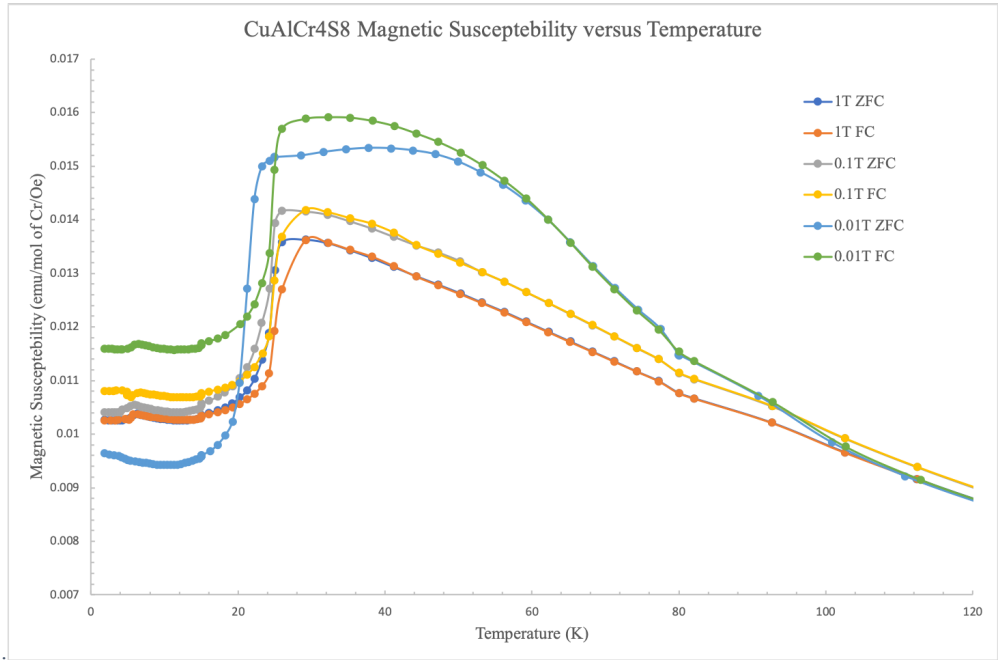

Figure 16: The same plot as in the previous figure with the x-axis scale enlarged to see low temperature behaviour.

The most interesting part of this plot is the large drop in the susceptibility at $T_c \approx 26K$. This rapid drop is interesting as it is characteristic of a potential first order phase transition, of which may be antiferromagnetic in nature. This transition was not present in the selenide sample, which leads me to speculate that the breathing phase may play an important factor in realizing this transition, however, further study of this material will be required. After this transition, the low temperature susceptibilities are hysteretic as well, with the difference in the FC and ZFC sets becoming very apparent in the weakest applied field. In general, the low field magnetic behaviour of this material is very rich. In addition, we also have some slight irreversibility, which is most evident in the lowest field where $T_{irr} \approx 58K$, indicating some spin freezing and glassy behaviour. As was present in the selenide sample, there is also another characteristic temperature $T_2 = 8K$, indicated by the kink in the curve. At high temperatures the expected Curie-Weiss behaviour is present. In non-frustrated magnets, there is typically an observable kink near the end of the Curie-Weiss fitted region at the Néel temperature [14], however, characteristic of frustration, the transition out of this region is smooth at around 80K. In order to determine the Curie-Weiss temperature, I plotted inverse susceptibility as a function of temperature, and conducted a linear fit of the Curie-Weiss region (see Figure 17).

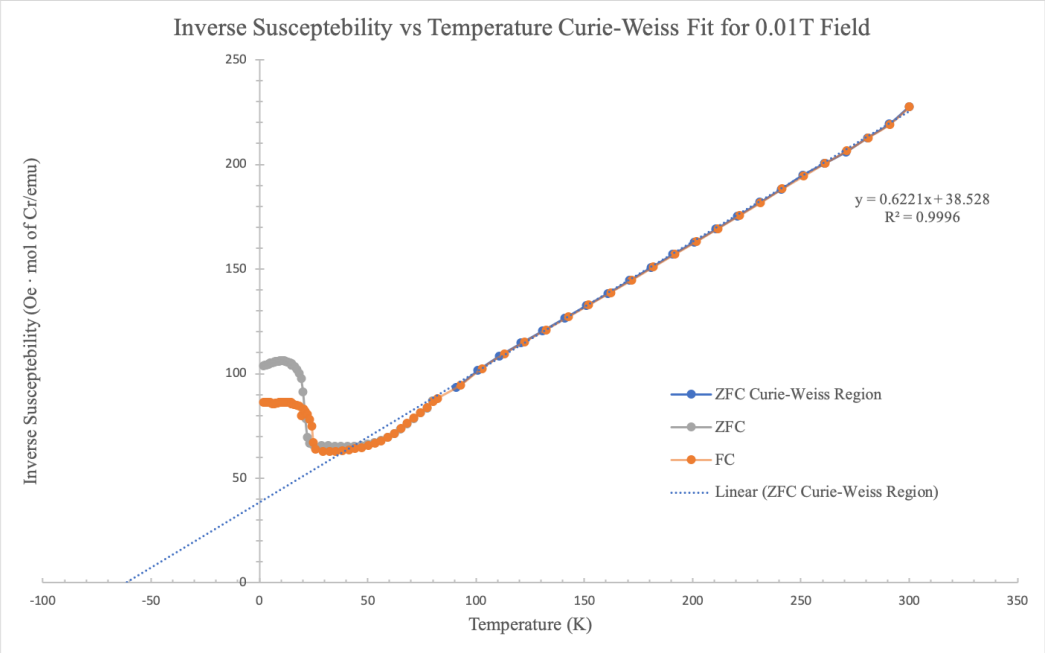

Figure 17: Plot of inverse susceptibility vs temperature in a 0.01T field with a Curie-Weiss fit of the linear region.

Using this plot, $\theta_{CW} = -61.93K$ can be obtained, of which, can then be used to calculate the frustration parameter $f = 0.420$, which appears quite low in comparison to breathing pyrochlore oxides [12]. I hypothesize that this is due to the difference in size between S and O, as the distances between the atoms in part dictate how strongly they interact. In our material θ_{CW} is small in comparison to $LiGaCr_4O_8$ (which was the structure used to refine our XRD data), where $\theta_{CW} = -658.8K$ [12]. This indicates that the interactions are far stronger in the oxide where the atoms are closer together. Supporting this prediction, value for θ_{CW} compares closely in magnitude with other breathing sulfides, as well as it is very close to that of $CuInCr_4S_8$ with $\theta_{CW} = -72K$ [16]. However, the magnetic behaviour of $CuInCr_4S_8$ ($B_f \approx 1.06$) was quite different compared to our material, especially in the

absence of a large susceptibility drop in the $CuInCr_4S_8$ M(T) plot [16]. However, another material, $LiInCr_4S_8$, almost has the same breathing factor (1.087 for our material vs approximate 1.09 for $LiInCr_4S_8$). Interestingly, $LiInCr_4S_8$ also undergoes a sharp drop in its susceptibility around the same temperature, however, it differs significantly in its Curie-Weiss temperature with $\theta_{CW} = 31K$. The difference in magnitude is not too great from our sample, however, the difference in sign indicates that while antiferromagnetic interactions may slightly dominate in $CuAlCr_4S_8$, ferro or ferrimagnetic interactions are more prevalent in LiInCr4S_8. Given the fact that very similar breathing factors both resulted in a significant drop in susceptibility, and possibly a first order phase transition, may be indicative of a structural transition. From Figure 17, I was also able to calculate $\mu_{eff} = 0.705\mu_B$, which differed from that of $LiInCr_4S_8$ with $\mu_{eff} = 1.168\mu_B$, which I calculated using the Curie constant C given in [16]. The effective moment of $CuAlCr_4S_8$, however, did compare quite closely with our selenide sample.

5 Conclusion

Overall, this investigation was able to produce very interesting results. The first reporting of the novel breathing pyrochlore $CuAlCr_4S_8$ is very exciting, as well as its magnetic behaviour is quite interesting. Going forward, the group will conduct further investigations to understand the nature of the transition involving the rapid drop in susceptibility. While this is strong evidence for a first order phase transition, a study of the heat capacity will be more conclusive, as a diverging heat capacity is characteristic of first order transitions. In

addition, the group will perform a temperature dependent XRD measurement to determine if a structural transition occurs. Also, more magnetic measurements should be carried out to fully characterize and understand the behaviour of this material. Measurements such as neutron diffraction and muon spin relaxation can be implemented to reveal more material properties. Overall, I think this thesis told an interesting story. Two nearly pure materials were synthesized, one with the breathing phase and one with site mixing. The presence of the breathing factor was shown to significantly alter magnetic behaviour of the material. However, it must also be accounted for in this comparison that S and Se differ in size as well, which could also significantly alter interactions. An example of this is shown through the difference in their respective Curie-Weiss temperatures. The effective magnetic moments, however, were quite similar. Given the number of materials attempted over the course of this project, it is safe to say that this is an elusive family of materials that are very difficult to experimentally realize. However, as this investigation has shown, this is a fruitful search, as the materials obtained exhibit rich and interesting physics. In the future, I think more synthesis attempts should be geared towards realizing a breathing pyrochlore with a different B-site atom, given that this is largely unexplored territory. It would be interesting to see if the group could find success in attempting some of the aforementioned failed materials, by swapping oxygen with sulfur, given that B-site elements of V, Mn, and Sc are chosen over Cr.

6 Bibliography

[1] D. J. Griffiths, *Introduction to Electrodynamics*, 4th ed. (Pearson, 2013).
[2] S. Blundell, *Magnetism in Condensed Matter* (Oxford, 2001).
[3] D. Griffiths and D. Schroeter, *Introduction to Quantum Mechanics*, 3rd ed. (Cambridge University Press, 2018).
[4] C. Kittel, *Introduction to Solid State Physics*, 8th ed. (John Wiley & Sons, Inc., 2005).
[5] L. Onsager, *Crystal Statistics. I. A Two-Dimensional Model with an Order-Disorder Transition*, Phys. Rev. **65**, 117 (1944).
[6] A. K. Murtazaev, D. R. Kurbanova, and M. K. Ramazanov, *Phase Transitions and Critical Properties of the Heisenberg Antiferromagnetic Model on a Body-Centered Cubic Lattice with Second Nearest Neighbor Interaction*, J. Exp. Theor. Phys. **129**, 903 (2019).
[7] K. Huang, *Introduction to Statistical Physics*, 2nd ed. (CRC Press Taylor & Francis Group, 2010).
[8] A. P. Ramirez, *Geometric Frustration: Magic Moments*, Nature **421**, 6922 (2003).
[9] J. S. Gardner, M. J. P. Gingras, and J. E. Greedan, *Magnetic Pyrochlore Oxides*, Rev. Mod. Phys. **82**, 53 (2010).
[10] L. Balents, *Spin Liquids in Frustrated Magnets*, Nature **464**, 7286 (2010).
[11] J. A. Mydosh, *Disordered Magnetism and Spin Glasses*, Journal of Magnetism and Magnetic Materials **157–158**, 606 (1996).
[12] Y. Okamoto, G. J. Nilsen, J. P. Attfield, and Z. Hiroi, *Breathing Pyrochlore Lattice Realized in A -Site Ordered Spinel Oxides LiGaCr 4 O 8 and LiInCr 4 O 8*, Phys. Rev. Lett. **110**, 097203 (2013).
[13] P. Ghosh, Y. Iqbal, T. Müller, R. T. Ponnaganti, R. Thomale, R. Narayanan, J. Reuther, M. J. P. Gingras, and H. O. Jeschke, *Breathing Chromium Spinels: A Showcase for a Variety of Pyrochlore Heisenberg Hamiltonians*, Npj Quantum Materials **4**, 1 (2019).
[14] C. Lacroix, P. Mendels, and F. Mila, editors , *Introduction to Frustrated Magnetism: Materials, Experiments, Theory* (Springer-Verlag, Berlin Heidelberg, 2011).
[15] G. Pokharel, H. S. Arachchige, T. J. Williams, A. F. May, R. S. Fishman, G. Sala, S. Calder, G. Ehlers, D. S. Parker, T. Hong, A. Wildes, D. Mandrus, J. A. M. Paddison, and A. D. Christianson, *Cluster Frustration in the Breathing Pyrochlore Magnet LiGaCr4S8*, Phys. Rev. Lett. **125**, 167201 (2020).
[16] Y. Okamoto, M. Mori, N. Katayama, A. Miyake, M. Tokunaga, A. Matsuo, K. Kindo, and K. Takenaka, *Magnetic and Structural Properties of A-Site Ordered Chromium Spinel Sulfides: Alternating Antiferromagnetic and Ferromagnetic Interactions in the Breathing Pyrochlore Lattice*, J. Phys. Soc. Jpn. **87**, 034709 (2018).
[17] L. E. Smart and E. A. Moore, *Solid State Chemistry An Introduction*, 3rd ed. (CRC Press Taylor & Francis Group, 2005).
[18] S. A. Speakman, *Basics of X-Ray Powder Diffraction*, 107 (2016).

[19] M. McElfresh, *Fundamentals of Magnetism and Magnetic Measurements Featuring Quantum Design's Magnetic Property Measurement System* (Quantum Design, Purdue University, 1994).
[20] N. Khaneja, *SQUID Magnetometers, Josephson Junctions, Confinement and BCS Theory of Superconductivity*, Magnetometers - Fundamentals and Applications of Magnetism (2019).
[21] H. L. Pinch, M. J. Woods, and E. Lopatin, *Some New Mixed A-Site Chromium Chalcogenide Spinels*, Materials Research Bulletin **5**, 425 (1970).
[22] J. G. Rau, L. S. Wu, A. F. May, A. E. Taylor, I.-L. Liu, J. Higgins, N. P. Butch, K. A. Ross, H. S. Nair, M. D. Lumsden, M. J. P. Gingras, and A. D. Christianson, *Behavior of the Breathing Pyrochlore Lattice Ba3Yb2Zn5O11 in Applied Magnetic Field*, J. Phys.: Condens. Matter **30**, 455801 (2018).
[23] J. Yan, X. Luo, F. C. Chen, Q. L. Pei, G. T. Lin, Y. Y. Han, L. Hu, P. Tong, W. H. Song, X. B. Zhu, and Y. P. Sun, *Anomalous Hall Effect in Two-Dimensional Non-Collinear Antiferromagnetic Semiconductor Cr0.68Se*, Appl. Phys. Lett. **111**, 022401 (2017).